JGP Journal of General Physiology

RESEARCH ARTICLE

Molecular determinants for agonist recognition and discrimination in P2X2 receptors

Federica Gasparri[1], Jesper Wengel[2], Thomas Grutter[3], and Stephan A. Pless[1]

P2X receptors (P2XRs) are trimeric ligand-gated ion channels that open a cation-selective pore in response to ATP binding. P2XRs contribute to synaptic transmission and are involved in pain and inflammation, thus representing valuable drug targets. Recent crystal structures have confirmed the findings of previous studies with regards to the amino acid chains involved in ligand recognition, but they have also suggested that backbone carbonyl atoms contribute to ATP recognition and discrimination. Here we use a combination of site-directed mutagenesis, amide-to-ester substitutions, and a range of ATP analogues with subtle alterations to either base or sugar component to investigate the contributions of backbone carbonyl atoms toward ligand recognition and discrimination in rat P2X2Rs. Our findings demonstrate that while the Lys69 backbone carbonyl makes an important contribution to ligand recognition, the discrimination between different ligands is mediated by both the side chain and the backbone carbonyl oxygen of Thr184. Together, our data demonstrate how conserved elements in P2X2Rs recognize and discriminate agonists.

Introduction

Adenosine triphosphate (ATP) is not only the major source of free energy in cells but also acts as a signaling molecule by directly activating P2X receptors (P2XRs), membrane-bound ion channels with cation-selective pores. The seven known receptor isoforms (P2X1–7R) form trimers and show widespread distribution in both neuronal and nonneuronal tissues and fulfill a variety of crucial functions. As a result, they have recently generated increasing attention as potential targets for drugs, e.g., analgesics, antiinflammatory agents, and antithrombotics (Jarvis et al., 2002; Hechler et al., 2005; Honore et al., 2006; Broom et al., 2008; Carter et al., 2009; Arulkumaran et al., 2011; Karasawa and Kawate, 2016). In this study, we focus on the P2X2 isoform, which has been implicated in nociception, sensory transduction (i.e., hearing), and neurotransmitter release (Burnstock, 2007; Khakh and North, 2012; Zhu et al., 2017).

To facilitate pharmacological targeting of these ligand-gated ion channels, the precise location and makeup of the orthosteric binding site has been investigated by a number of mutagenesis studies (Ennion et al., 2000; Jiang et al., 2000; Roberts and Evans, 2004, 2006; Zemkova et al., 2007; Chataigneau et al., 2013). In combination with structural data, it has been possible to firmly establish an extracellular pocket located at the interface of two adjacent subunits as the ATP-binding site (Wilkinson et al., 2006; Marquez-Klaka et al., 2009; Hattori and Gouaux, 2012; Hausmann et al., 2015). Interestingly, the sequence of side chains lining this pocket does not resemble that of other more commonly encountered ATP-binding motifs, such as Walker or C (Walker et al., 1982; Freist et al., 1998), further emphasizing the need for a detailed understanding of what contributes to the recognition and discrimination of ligands by this noncanonical ATP-binding site.

The orthosteric ligand binding site is lined by a number of conserved side chains from two adjacent subunits (Lys69, Lys71, Thr184, Lys188, Arg290, Lys308, and Asn296, rat P2X2R numbering). While the involvement of these side chains has been confirmed in a number of P2XR subtypes (Ennion et al., 2000; Jiang et al., 2000; Zemkova et al., 2007; Roberts et al., 2008; Chataigneau et al., 2013; Hausmann et al., 2013), recent structural work (Hattori and Gouaux, 2012; Mansoor et al., 2016) suggested that some positions (Lys69 and Thr184) make contact with ATP via both their side chains and their backbone carbonyl oxygen atoms. However, it has not been possible to confirm these notions experimentally, as conventional mutagenesis does not allow for alterations of the protein backbone. Additionally, only limited data are available on ATP analogues containing subtle alterations to either their ribose sugar or purine base

[1]Center for Biopharmaceuticals, Department of Drug Design and Pharmacology, University of Copenhagen, Copenhagen, Denmark; [2]Biomolecular Nanoscale Engineering Center, Department of Physics, Chemistry and Pharmacy, University of Southern Denmark, Odense, Denmark; [3]University of Strasbourg, Centre National de la Recherche Scientifique, Conception et Application de Molécules Bioactives Unité Mixte de Recherche 7199, Strasbourg, France.

Correspondence to Stephan A. Pless: stephan.pless@sund.ku.dk; F. Gasparri's present address is Dept. of Biosciences, University of Milan, Milan, Italy.

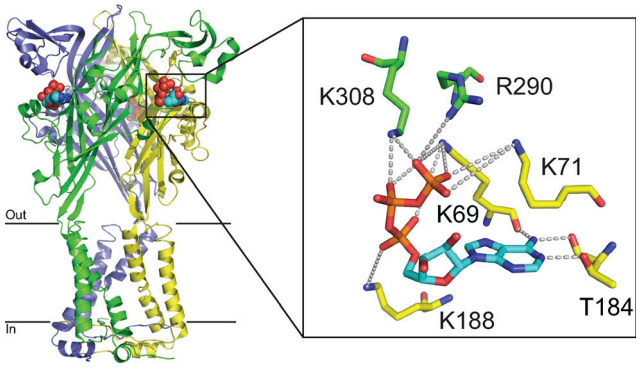

Figure 1. **Overview of P2XR structure and close-up view of the orthosteric binding site.** X-ray crystal structure of the ATP-bound human P2X3R (PDB accession no. 5SVK), with individual subunits color coded and black bars representing approximate boundaries of the cell membrane. Inset shows conserved hydrophilic side chains and backbone carbonyls suggested to interact with ATP (rP2X2R numbering), as indicated by dotted lines.

components. This has limited our understanding of what interactions contribute to the recognition of ATP and/or discrimination between nucleoside triphosphate analogues. The latter is of physiological relevance, because other nucleoside triphosphates (e.g., uridine 5′-triphosphate [UTP]) can be coreleased at purinergic synapses and can directly activate some P2XRs (Lazarowski et al., 2003).

Further, previous studies have shown that when P2X2Rs open, they show a high degree of channel flicker (Evans, 1996; Ding and Sachs, 1999), suggesting the existence of multiple open states between which the protein rapidly interconverts. However, it is not yet known if the relative occupancy of these states (i.e., the channel flicker) is determined by the chemical composition of the ligand in the orthosteric binding site.

In this study, we therefore (a) employ the nonsense suppression method to introduce amide-to-ester substitutions in the rat P2X2 receptor (rP2X2R) ATP-binding site, (b) systematically test a range of six base- and seven sugar-modified nucleoside triphosphate analogues to elucidate agonist discrimination, and (c) use single channel analysis to assess possible effects of ligand structure on the relative occupancy of open channel states, which ATP-activated P2XRs rapidly flicker between. Together, our results unambiguously demonstrate the important functional contribution of backbone-mediated H-bonds at Lys69 and Thr184, as well as provide a detailed picture of how interactions of the ribose sugar and purine/pyrimidine base contribute to ligand recognition and discrimination.

Materials and methods

Chemicals

All salts were purchased from Sigma-Aldrich. Cytidine 5′-triphosphate (CTP; purity 95%); UTP (purity 90%); and guanidine 5′-triphosphate (GTP; purity 90%), used for single-channel experiments, were obtained from Acros Organics (Thermo Fisher Scientific). Inosine 5′-triphosphate (ITP; purity 98%), 6-chloropurineriboside-5′-triphosphate (6-Cl–rTP; purity 90%), 2′-fluoro-2′-deoxyadenosine-5′-triphosphate (C2′-F-dATP; purity 95%), 3′-deoxyadenosine-5′-triphosphate (C3′-dATP; purity 90%), and 2′,3′-dideoxyadenosine-5′-triphosphate (C2′-C3′-ddATP; purity 95%) were purchased from TriLink Biotechnologies. Adenosine 5′-triphosphate (ATP; purity 99%), GTP, used for two-electrode voltage clamp experiments (purity 95%), and 2′-deoxyadenosine-5′-triphosphate (C2′-dATP; purity 98%) were from Sigma-Aldrich. isoGTP (purity 93–95%) was purchased from Chemgenes, while Ara-adenosine 5′-triphosphate (Ara-ATP; purity 96%) was from IBA Lifesciences. Last, locked nucleic acid–ATP (LNA-ATP) and unlocked nucleic acid–ATP (UNA-ATP) were provided by J. Wengel (University of Southern Denmark, Odense, DK).

Expression of P2X2R in *Xenopus laevis* oocytes

The complementary DNA of the rP2X2R, subcloned into the pNKS2 vector, was used for standard site-directed mutagenesis with custom-designed primers (Eurofins Genomics) and PCR with PfuUltra II Fusion HS DNA polymerase (Agilent Technologies). The naturally occurring amber TAG stop codon at the end of the coding frame was mutated to a TAA stop codon to allow for specific incorporation of ncAAs (non-canonical amino acids) using a TAG stop codon. Complementary DNA was first linearized with Xho I (New England Biolabs) and subsequently transcribed to messenger RNA (mRNA) with the Ambion mMessage mMACHINE SP6 transcription kit (Thermo Fisher Scientific) and purified with RNeasy columns (Qiagen). The nonsense suppression method, relying on the enzymatic in vitro aminoacylation of a synthetic *Tetrahymena thermophila* transfer RNA (tRNA), which naturally recognizes the amber TAG stop codon (Saks et al., 1996; Nowak et al., 1998), was used for the incorporation of 2-hydroxyisovaleric acid (Vah). tRNA was synthetized and aminoacylated as previously described (Lynagh et al., 2017). Briefly, double-stranded DNA strands (Integrated DNA Technologies) were used as templates for RNA synthesis with the T7-Scribe transcription kit (Cellscript) and purified with Chroma Spin DEPC-H2O columns (Clontech). tRNA aminoacylation with Vah was performed in vitro using T4DNA ligase (New England Biolabs), and the aminoacylated tRNA was purified with phenol-chloroform extraction and ethanol precipitation. The pellet was air-dried and stored at −80°C until use. Oocytes from *X. laevis* frogs (anesthetized in 0.3% tricaine, according to license 2014-15-0201-00031, approved by the Danish Veterinary and Food Administration) were digested with collagenase (1.5 mg/ml; Roche) dissolved in OR2 (in mM: 82 NaCl, 2.5 KCl, 1 $MgCl_2$, and 5 HEPES, adjusted to pH 7.4 with NaOH) with continuous shaking. Oocytes were incubated in OR2 at 18°C until injection of mRNA. WT (30 ng in a volume of 9.2 nl) and mutant (1–4 µg in a volume from 13.8 nl to a maximum 50.6 nl) rP2X2R mRNAs were injected with a Nanoliter 2010 injector (World Precision Instruments) into the oocyte cytoplasm. For Vah incorporation, aminoacyl-tRNA was resuspended in 1 µl of ice-cold water immediately before coinjection with 2 µg of TAG-containing mutant mRNA in a total volume of 50 nl (note that TAG is UAG in RNA). tRNA enzymatically ligated to only the dinucleotide phosphodesoxy-cytosine phospho-adenosine was also resuspended in 1 µl of ice-cold water and coinjected with the same TAG-containing mutant mRNA as a negative control.

Injected oocytes were incubated in Leibovitz's L-15 medium (Life Technologies) with 5 mM L-glutamine, 2.5 mg/ml gentamycin, and 15 mM HEPES (pH 7.6 with NaOH) and gently shaken at 18°C until experiments.

Two-electrode voltage clamp recordings and data analysis

One to two days after mRNA injection, oocytes were placed into a custom-made chamber (Dahan et al., 2004) and perfused with ND96 solution (in mM: 96 NaCl, 2 KCl, 1.8 $BaCl_2$, 1 $MgCl_2$, and 5 HEPES, pH 7.4) through an automated perfusion system operated by a ValveBank module (AutoMate Scientific). All agonist-containing solutions were freshly prepared before recordings, dissolved in ND96, and pH-adjusted to 7.4 with NaOH and/or HCl. Oocytes were clamped at −40 mV. Currents were recorded with microelectrodes (resistance of 0.3–2 MΩ; Harvard Apparatus) filled with 3 M KCl and an Oocyte Clamp C-725C amplifier (Warner Instrument Corp.). Current traces were acquired at 500-Hz via an Axon Digidata 1550 interface and Clampex 10.5.1.0 software (Molecular Devices). The signal was further analyzed in Clampfit 10 (Molecular Devices) and digitally filtered at 10 Hz with an eight-pole Bessel filter for analysis and display. Agonist-elicited concentration–response curves were obtained by normalization of agonist-induced responses and subsequently fitted to a one-component Hill equation in Prism v7 (GraphPad) to calculate half maximal effective agonist concentration (EC_{50}) values and Hill coefficients. Relative efficacy, described in percentage, was determined by comparing the maximal current elicited by the agonist in question with that elicited by a saturating concentration of ATP (on the same cell). Data analysis was performed using Prism v7, and significant differences were determined by one-way ANOVA with Dunnett's test. Statistical significance between maximal current elicited by ncAA-containing P2X2Rs and the corresponding negative control was established using an unpaired Student's *t* test.

Cell culture and transfection

HEK-293 cells were grown in Dulbecco's modified Eagle's medium supplemented with 10% fetal bovine serum (Invitrogen), 100 U/ml penicillin, and 100 µg/ml streptomycin (Invitrogen) and incubated at 37°C with 5% CO_2. After PBS wash, trypsin-treated cells (Trypsine-EDTA; Thermo Fisher Scientific) were resuspended in Dulbecco's modified Eagle's medium and seeded onto glass coverslips pretreated with poly-L-lysine in 35-mm dishes. Transfection was performed by using the calcium phosphate precipitation method. rP2X2-3T DNA (0.05 µg; Li et al., 2008; Jiang et al., 2010) was mixed with DNA coding for GFP (0.3 µg) to identify cells that were positively transfected (Habermacher et al., 2016). 1 d after transfection, cells were washed with fresh medium, and recordings were performed within 24 h.

Table 1. **ATP-elicited concentration–response data for Lys69, 71, 188, and 308 and Arg290 mutants**

rP2X2 construct	EC_{50} (µM)	n_H	*n*
WT	32 ± 4	1.4 ± 0.1	15
Lys69Arg	6,000 ± 500****	1.2 ± 0.1	13
Lys69Gln	16,600 ± 550****	2.4 ± 0.1****	10
Val70Vah	120 ± 2	1.6 ± 0.1	12
Val96Vah	27 ± 2	1.7 ± 0.1	6
Lys71Arg	370 ± 40	1.1 ± 0.1	12
Lys71Gln	6,300 ± 400****	1.4 ± 0.1	15
Lys188Arg	57 ± 8	1.1 ± 0.1**	13
Lys188Gln	8,700 ± 500****	1.7 ± 0.1	16
Lys308Arg	6,000 ± 400****	0.8 ±0.1****	24
Lys308Gln	5,800 ± 700****	1.1 ±0.1	13
Arg290Lys	460 ± 60	1 ± 0.1**	7
Arg290Gln	4,900 ± 500****	1.1 ± 0.1**	15

ATP-elicited concentration–response data (EC_{50}) and Hill coefficient (n_H; shown as mean ± SEM), as well as number of experiments (*n*) for WT and mutants of conserved basic amino acids (including Val70Vah and Val96Vah amide-to-ester mutant, the latter serving as a control for Vah incorporation). Significant differences were determined by one-way ANOVA with Dunnett's test. **, P < 0.01; ****, P < 0.0001.

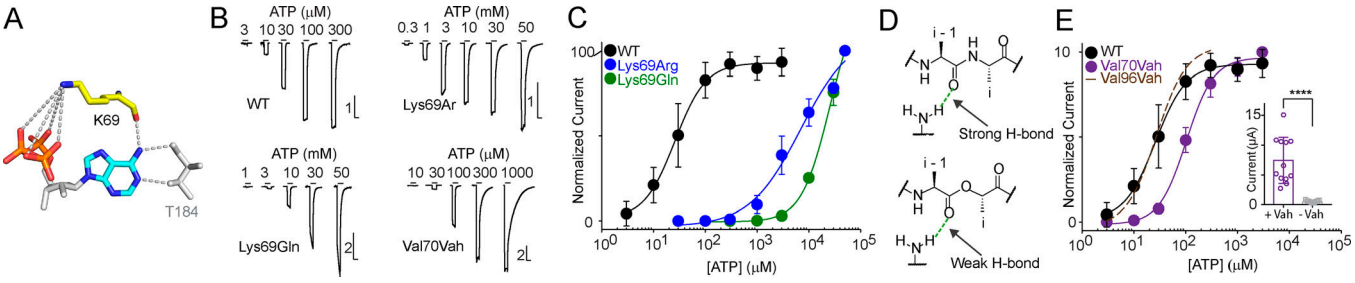

Figure 2. **The role of Lys69 side chain and backbone carbonyl in ATP recognition. (A)** Closeup of the ATP-binding pocket with dotted lines indicating proposed interactions between ATP and Lys69. **(B and C)** Example recordings (B) and ATP-elicited concentration–response data (C) for WT and mutant P2X2Rs in response to increasing concentrations of ATP. Bars in B, x, 15 s; y, µA; data in C displayed as mean ± SD (*n* = 10–15). **(D)** Schematic showing the reduced H-bond acceptor propensity as a result of amide-to-ester substitutions. **(E)** ATP-elicited concentration–response data for WT and Val70Vah and Val96Vah mutants (the latter serving as a control for Vah incorporation). Inset represents the mean peak current amplitude (± SD) elicited by 3 mM ATP at oocytes injected with Val70TAG mRNA and uncharged (−Vah) or charged (+Vah) tRNAs (*n* = 6–12; ****, P < 0.0001; Student's *t* test).

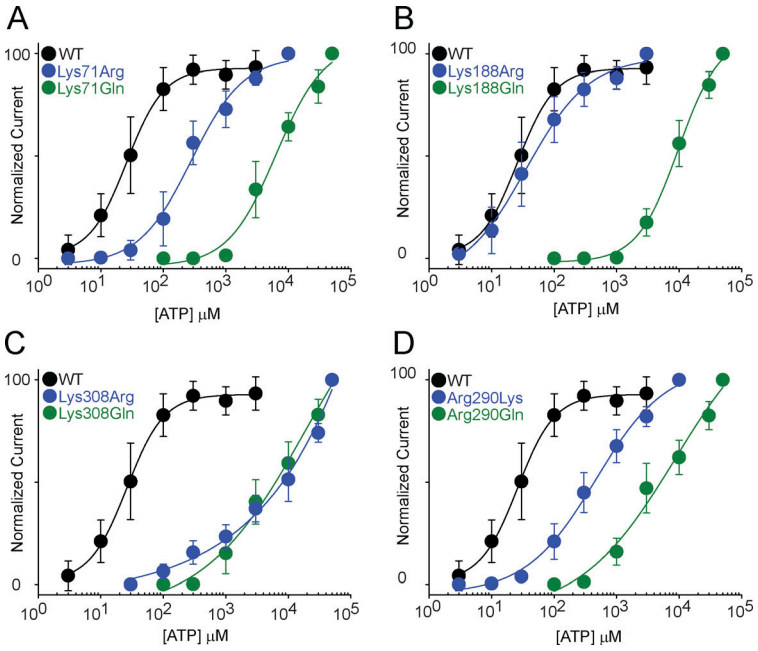

Figure 3. **Differential effects of charge-retaining and -neutralizing mutations at other conserved basic side chains lining the orthosteric binding site. (A–D)** ATP-elicited concentration–response data for WT, and Lys/Arg/Gln mutants at positions Lys71, Lys188, Lys308, and Arg290 (mean ± SD; *n* = 7–24).

Single channel patch-clamp recordings and data analysis

HEK-293 cells were used for single-channel recordings in the outside-out patch configuration. Borosilicate capillaries (Harvard Apparatus) were pulled by using a horizontal micropipette puller (model p-97; Sutter Instruments) and coated with Sylgrad 184 (Dow Corning Co.). Patch pipettes (resistance of 7–20 MΩ) containing (in mM) 147 NaF, 10 EGTA, and 10 HEPES adjusted to pH 7.3 were used. Outside-out patches were pulled according to standard procedure. Once a stable patch was obtained, the holding potential was set to −120 mV through an EPC-10 amplifier (HEKA), while data were acquired at 4 kHz and low-pass filtered at 2.9 kHz via PatchMaster software (HEKA). Extracellular solution (in mM: 147 NaCl, 2 KCl, 1 $CaCl_2$, 1 $MgCl_2$, 10 HEPES, and 13 glucose, pH 7.3 [NaOH], mOsmol/kg 280–300; either containing or not containing ATP/other agonists) was delivered through a three-tube perfusion system (SF77A Perfusion Fast step; Warner), which allowed fast solution exchange (5–10 ms), once placed in front of the patch pipette. Sweeps of 12 s were run, and ATP/other agonists were applied for 10 s with an interval of 1 min to allow for washout and recovery.

Data acquired were analyzed offline using the TAC software (Bruxton Corp.). Sweeps with a stable baseline and minimal leak current were refiltered to obtain a cascade filter corner frequency of 1 kHz. Channel events and conductance levels were measured by all-points amplitude histograms fitted to Gaussian distributions. Data collected from a minimum of 5 to a maximum of 20 patches were averaged and plotted as mean ± SD. The unpaired Student's *t* test was used to determine statistical significance differences.

Results

Lys69 forms strong side chain– and weak backbone-mediated H-bonds with ATP and CTP

Recent crystal structures of ATP-bound P2XRs have confirmed the previously proposed close proximity between conserved basic side chains (Lys69, Lys71, Lys188, Arg290, and Lys308) and the negatively charged phosphate tail of ATP (Fig. 1; Hattori and Gouaux, 2012; Kasuya et al., 2016, 2017; Mansoor et al., 2016), strongly suggesting these charge–charge interactions to be crucial for ligand binding. Interestingly, the structural data also indicated a dual role for Lys69: while the side chain amine of Lys69 is poised to interact with the ATP phosphate tail, the backbone carbonyl oxygen is likely to form an H-bond with the ATP C6-amine substituent (Fig. 2 A). We thus set out to functionally probe the individual contributions of both the Lys side chain amine and the carbonyl oxygen to ATP recognition. To this end, we first mutated Lys69 to both Arg and Gln and assessed the resulting phenotype using a two-electrode voltage clamp in *Xenopus* oocytes. As predicted from previous work on P2X1Rs (Ennion et al., 2000) and P2X2Rs (Jiang et al., 2000; Chataigneau et al., 2013; Mansoor et al., 2016), both mutations were detrimental to ATP-induced currents; the charge-preserving Arg replacement resulted in nearly as large a right-shift in EC_{50} as the charge-neutralizing Gln mutation (EC_{50} values over 5 mM for both mutants; Fig. 2, B and C; and Table 1). This strongly suggests that both side chain geometry and/or H-bond pattern are critical to ATP recognition in this position (similar to Lys308 mutants, while Lys71, Lys188, and Arg290 mutants display divergent patterns; Fig. 3 and Table 1).

Next, and in order to assess the contribution of the predicted backbone-mediated H-bond with ATP, we replaced the adjacent Val70 with the α-hydroxy analogue Vah using the nonsense suppression methodology (Nowak et al., 1998; England et al., 1999). Incorporating such a noncanonical amino acid replaces the backbone amide with a backbone ester bond, thus significantly reducing, but not eliminating, the H-bond acceptor propensity of the backbone carbonyl at the preceding position (Sereikaitė et al., 2018; Fig. 2 D). It is therefore important to point out that results obtained with this type of backbone manipulation likely underestimate the full contribution of the backbone-mediated H-bonds.

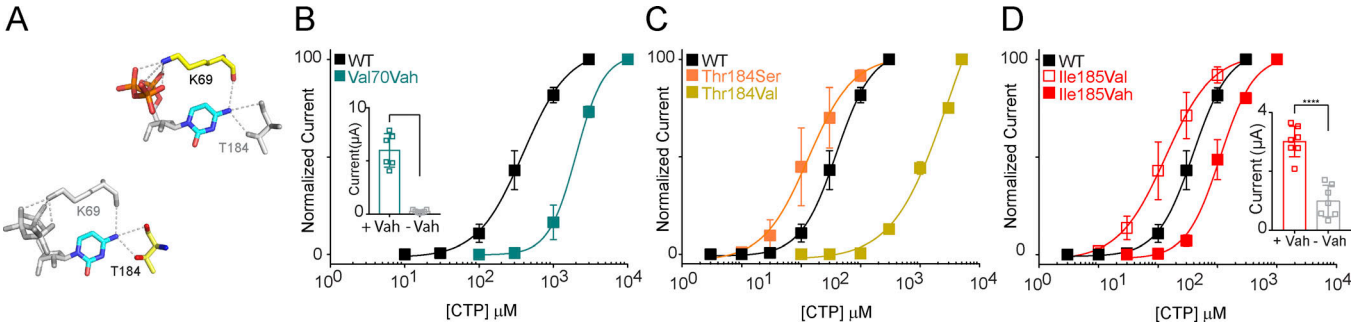

Figure 4. **Role of side chain- and backbone-mediated H-bonds in CTP recognition. (A)** Closeup of the ATP-binding pocket with dotted lines indicating proposed interactions between CTP and Lys69 (upper panel) and Thr184 (lower panel). **(B–D)** CTP-elicited concentration–response data for WT and Val70Vah (B), WT, Thr184Ser, and Thr184Val (C), and WT, Ile185Val, and Ile185Vah (D; mean ± SD; n = 6–8). Insets show the mean peak current amplitude (±SD) elicited by 10 mM CTP at oocytes injected with Val70TAG (B) or Ile185TAG (D) mRNA and uncharged (–Vah) or charged (+Vah) tRNAs, respectively (n = 6–7; ****, $P < 0.0001$; Student's t test).

Backbone ester incorporation, via synthetic tRNAs charged with Vah (Pless and Ahern, 2013), led to robust macroscopic currents and a modest (fourfold) increase in ATP EC_{50} (Fig. 2, B and E; and Table 1). To confirm the specific incorporation of Vah, we performed control experiments using uncharged tRNAs (i.e., not carrying Vah). This did not result in significant ATP-gated currents and thus validated the results obtained with Vah (inset, Fig. 2 E). To test for possible nonspecific effects of Vah incorporation on channel function, we inserted Vah in position 96 (located on an adjacent loop). This did not affect the ATP EC_{50} (Fig. 2 E).

In addition to the primary endogenous agonist ATP, P2X2Rs can be activated by other nucleoside triphosphates (Coddou et al., 2011; Browne and North, 2013), raising the question of whether the backbone-mediated H-bond is also crucial for the recognition of other agonists. Indeed, recent structural work on CTP-bound P2X4Rs from zebrafish had proposed a similar role for Lys69 in the recognition of CTP, i.e., for the side chain amine to coordinate the phosphate tail of CTP, while the backbone carbonyl was suggested to form a H-bond with the CTP C4-amine substituent (Kasuya et al., 2017), which is equivalent to the purine C6-amine substituent of ATP. Based on the slightly longer distance for the latter interaction compared with that in the ATP-bound structure, it had been suggested that this may, at least in part, account for the lower potency of CTP compared with ATP. To test this notion experimentally, we compared CTP-activated currents in both WT and Vah70 channels (Fig. 4). As expected, CTP displays a roughly 10-fold lowered apparent affinity compared with ATP (EC_{50} 370 ± 30 μM versus 32 ± 4 μM). However, and similar to the relative increase in EC_{50} observed for ATP, Vah70 channels showed a fivefold right-shift in the CTP concentration–response curve (Table 2), suggesting a similar relative contribution of the backbone-mediated H-bond to the recognition of both ligands.

Thr184 forms interactions with ATP and CTP via both side chain and backbone

In analogy to the dual role in ligand recognition by Lys69, Thr184 had been suggested to contribute to recognition of ATP through both side chain– and backbone-mediated H-bonds (Hattori and Gouaux, 2012; Mansoor et al., 2016; Fig. 5 A). We thus set out to probe this prediction experimentally by replacing the Thr184

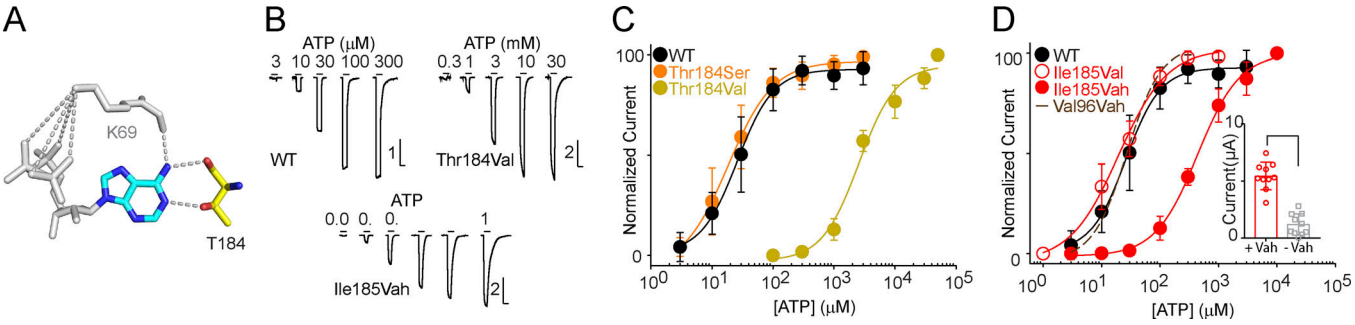

Figure 5. **The role of Thr184 side chain and backbone carbonyl in ATP recognition. (A)** Closeup of the ATP-binding pocket with dotted lines indicating proposed interactions between ATP and Thr184. **(B and C)** Example recordings (B) and ATP-elicited concentration–response data (C) for WT and mutant P2X2Rs in response to increasing concentrations of ATP. Bars in B, x, 15 s; y, μA; data in C displayed as mean ± SD (n = 14–25). **(D)** ATP-elicited concentration–response data for WT, Ile185Vah, Ile185Val, and Val96Vah mutants (the latter serving as a control for Vah incorporation). Inset represents the mean peak current amplitude (±SD) elicited by 10 mM of ATP in oocytes injected with Ile185TAG mRNA and uncharged (–Vah) or charged (+Vah) tRNAs (n = 7–10; ****, $P < 0.0001$, Student's t test).

Table 2. **Concentration–response data for CTP-gated currents at different mutants**

rP2X2 construct	EC_{50} (μM)	n_H	*n*
WT	370 ± 30	1.7 ± 0.2	7
Val70Vah	2,000 ± 90****	2.6 ± 0.1****	6
Thr184Ser	156 ± 30	1.5 ± 0.1	6
Thr184Val	11,700 ± 300****	1.6 ± 0.1	8
Ile185Val	144 ± 30	1.3 ± 0.1	6
Ile185Vah	1,100 ± 80*	1.7 ± 0.1*	7

CTP-elicited concentration–response data (EC_{50}) and Hill coefficient (n_H; shown as mean ± SEM), as well as number of experiments (*n*) for WT, the conventional Thr184Ser, Thr184Val, Ile185Val, and the Val70Vah/Ile185Vah amide-to-ester mutants. Significant differences were determined by one-way ANOVA with Dunnett's test. *, P ≤ 0.01; ****, P < 0.0001.

Table 3. **ATP-elicited concentration–response data for Thr184 mutants**

rP2X2 construct	EC_{50} (μM)	n_H	*n*
WT	32 ± 4	1.4 ± 0.1	15
Thr184Ser	26 ± 3	1.4 ± 0.1	25
Thr184Val	3,200 ± 200****	1.3 ± 0.1	14
Ile185Val	23 ± 3	1.3 ± 0.1	10
Ile185Vah	460 ± 20**	1.3 ± 0.1	10
Val96Vah	27 ± 2	1.7 ± 0.1	6

ATP-elicited concentration–response data (EC_{50}) and Hill coefficient (n_H; shown as mean ± SEM), as well as number of experiments (*n*) for WT and Thr184/Ile185 mutants, including the Ile185Vah and Val96Vah amide-to-ester mutants (the latter served as a control for Vah incorporation). Significant differences were determined by one-way ANOVA with Dunnett's test. **, P < 0.01; ****, P < 0.0001.

side chain, as well as introducing an amide-to-ester substitution in position 185 in order to reduce the H-bonding propensity of the backbone carbonyl at position 184. First, we replaced Thr184 with Val, which is isosteric to Thr, but cannot engage in H-bonds. This led to a drastic (100-fold) reduction in sensitivity to ATP. By contrast, the Thr184Ser mutation, which maintains the ability for H-bonding, resulted in WT-like sensitivity to ATP (Fig. 5, B and C; and Table 3). This clearly demonstrated that it is the Thr184 hydroxyl that is crucial to ATP recognition. Next, we introduced Vah in position 185 in order to probe the proposed contribution of the backbone carbonyl to ATP recognition (Vah was used instead of the α-hydroxy acid of Ile, as the conventional Ile185Val did not affect receptor function: EC_{50} = 23 ± 3 μM, *n* = 10; Table 3). This led to a pronounced (20-fold) decrease in ATP sensitivity (compared with Ile185Val), thus confirming the crucial role of this backbone-mediated H-bond (Fig. 5 D and Table 3).

To assess if both Thr184-mediated interactions are conserved for CTP, we obtained CTP-induced concentration–response data for the Thr184Ser, Thr184Val, and Ile185Vah mutants. While the Thr184Val mutation right-shifted the CTP EC_{50} by ∼30-fold (compared with 100-fold for ATP), the Val-to-Vah substitution in position 185 increased the EC_{50} eightfold (compared with 20-fold for ATP; Fig. 4 and Table 2). These less pronounced effects by the mutations likely reflect the fact that the CTP pyrimidine base is smaller and thus likely not ideally positioned to interact with both the backbone carbonyl and the side chain hydroxyl of Thr184. By contrast, the backbone carbonyl in position 69 appears to make similar contributions to both ATP and CTP recognition.

Together, our data clearly underline the importance of the backbone-mediated H-bonds at Lys69 and Thr184 in the recognition of different nucleoside triphosphates by P2X2Rs and point to a crucial role for the Thr184 backbone carbonyl oxygen in agonist discrimination.

Probing base-modified P2X2R agonists

The differential impact of binding site mutations observed for different nucleoside triphosphate ligands (ATP versus CTP) led us to probe the contribution of base-modified agonists using WT P2X2Rs in more detail. To this end, we assembled a range of nucleoside triphosphate analogues that differed from either ATP or CTP in only one or two positions of the base (Fig. 6, A and B). As even relatively bulky substituents have been shown to be well tolerated on the purine C8 position (Jiang et al., 2011), we focused on C2- and C6-substituents of purine and the equivalent C2- and C4-substituents of pyrimidine analogues, respectively.

First, we aimed to complement our above experiments on the contribution of backbone-mediated H-bonds with the purine C6-amino substituent of ATP by using analogues that differed in mainly the C6-substituent, namely 6-Cl–rTP and ITP (Fig. 6 B). Consistent with the notion of the purine C6-amino substituent of ATP forming two important interactions with backbone carbonyl oxygens (Lys69 and Thr184), replacing this C6-amino substituent with chlorine (6-Cl–rTP) or a carbonyl oxygen (ITP) led to a strong decrease in apparent agonist affinity. While application of 6-Cl–rTP elicited currents in WT P2X2Rs, we could not confidently fit the data to obtain a reliable EC_{50} (Fig. 6 C and Table 4), as the cost of the compound prevented us from using concentrations above 500 μM. However, it is apparent that the EC_{50} is significantly increased compared with ATP. ITP contains a C6-carbonyl oxygen substituent and failed to evoke any currents at concentrations of up to 1 mM (Fig. 6, B and C; and Table 4). Similarly, isoGTP, which maintains the purine C6-amino substituent of ATP but harbors an additional C2-carbonyl oxygen substituent (no C2 substituent is present in ATP), only elicited very small currents at WT P2X2Rs at concentrations of up to 300 μM (Fig. 6, B and C; and Table 4). This indicated that the presence of a substituent in the 2 position alone decreases the ability of the agonist to activate WT P2X2Rs (EC_{50} ≥100-fold increased, as we cannot exclude the possibility of direct activation by isoGTP at higher concentrations). Consistent with the above notion regarding the C2 substutuent, GTP, which carries reversed C2- and C6-substituents compared with isoGTP (i.e., C6-carbonyl oxygen and C2-amino), showed both low efficacy and low apparent affinity at WT P2X2Rs (Fig. 6, B and C; and Table 4).

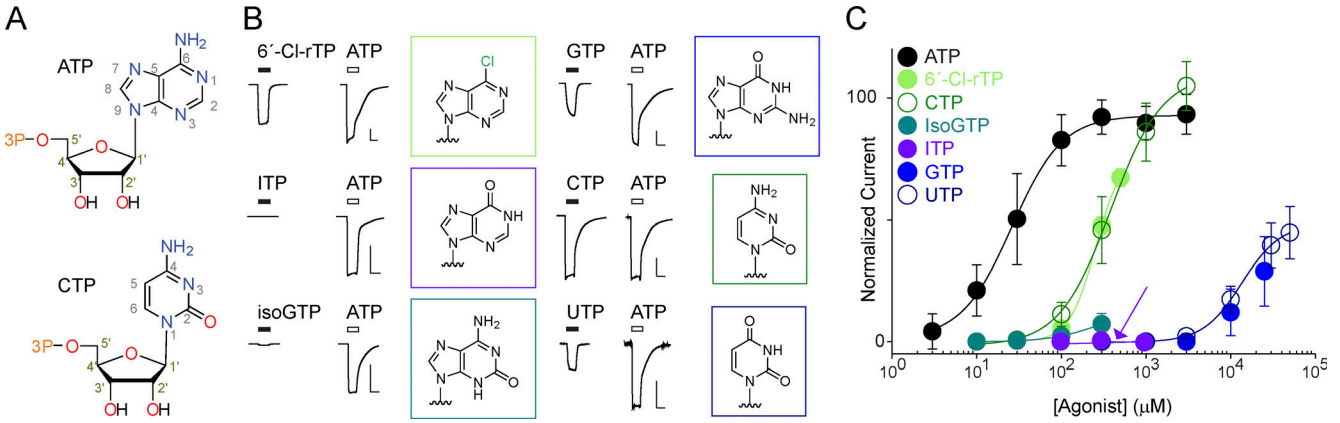

Figure 6. **Probing the effects of base modifications on ligand recognition. (A)** Chemical structure of ATP (upper structure) and CTP (lower structure). **(B)** Peak current recorded in response to the highest tested concentration of base-modified nucleoside triphosphate analogues (chemical base structures shown in frames), compared with that elicited by 1 mM of ATP. Bars, x, 12 s; y, 2 µA. **(C)** ATP-elicited concentration–response data for base-modified analogues, normalized to current elicited by 1 mM of ATP (mean ± SD; *n* = 5–15). Arrow indicates data for ITP. Note that the cost of 6-Cl–rTP, ITP, isoGTP, and GTP prevented us from using higher concentrations than those stated in the text (data for GTP could not be reliably fit).

Together, the purine analogues (6-Cl–rTP, ITP, isoGTP, and GTP) have demonstrated the importance of C2- and C6-substituents for both efficacy and apparent affinity. Next, we turned to pyrimidine analogues in order to assess the impact of C2- and C4-substituents in these smaller bases (equivalent to C2- and C6-purine substituents). Consistent with pyrimidine bases occupying less space in the ligand-binding pocket than purine-based analogues, we observed that maintaining the pyrimidine C4-amino group and only adding a C2-carbonyl oxygen (CTP) did not alter efficacy, but reduced the apparent affinity ∼12-fold (Fig. 6, B and C; and Table 4). Even UTP, which has not only a C2- but also a C4-carbonyl oxygen, was still able to activate P2X2Rs, albeit with 400-fold reduced apparent affinity and significantly reduced efficacy (Fig. 6, B and C; and Table 4). This reiterates the importance of pyrimidine C2- and C4-substituents for both efficacy and apparent affinity, but suggests a greater tolerance for substituents in these positions, likely due to smaller size of the pyrimidine bases.

Probing ribose-modified P2X2R agonists

Next, we aimed at testing a range of ribose-modified ATP analogues in order to assess the effect of adding or removing conformational restraints on the ribose ring, as well as removing or replacing the C2′ and C3′ ribose hydroxyl groups.

In light of the proposed U-shaped binding pose of ATP (Hattori and Gouaux, 2012; Fryatt et al., 2016; Mansoor et al., 2016) and the ability of ribose sugars to alternate between C2′-endo and C3′-endo conformations (Fig. 7 A), we tested whether conformational restraint on the ribose sugar would affect apparent affinity and/or efficacy. We thus first employed a less restrained sugar analogue, UNA-ATP (Campbell and Wengel, 2011), which lacks a covalent bond between the C2′ and C3′ ring positions. This analogue failed to elicit macroscopic currents, even at high (1 mM) concentrations, suggesting that a covalent link between the C2′ and C3′ ring positions is required for channel opening, likely in order to confer a degree of structural rigidity in the ligand (Fig. 8).

Table 4. **Concentration–response data for different base-modified agonists**

Agonist	EC_{50} (µM)	n_H	$I_{max\ agonist}/I_{max\ ATP}$(%)	*n*
ATP	32 ± 4	1.4 ± 0.1	n/a	15
CTP	370 ± 30	1.7 ± 0.1	105 ± 4	7
6-Cl–rTP	>300	ND	ND	5
ITP	ND	ND	ND	11
isoGTP	ND	ND	ND	10
GTP	ND	ND	ND	8
UTP	12,000 ± 480****	2.6 ± 0.2****	45 ± 3	11

Concentration–response data (EC_{50}) and Hill coefficient (n_H) for ATP and a range of base-modified nucleoside triphosphate analogues (shown as mean ± SEM). Relative efficacy expressed as maximal current compared to that elicited by 1 mM of ATP and number of experiments (*n*) and are also shown (n/a: not applicable; ND, not determined). Significant differences were determined by one-way ANOVA with Dunnett's test. ****, P < 0.0001.

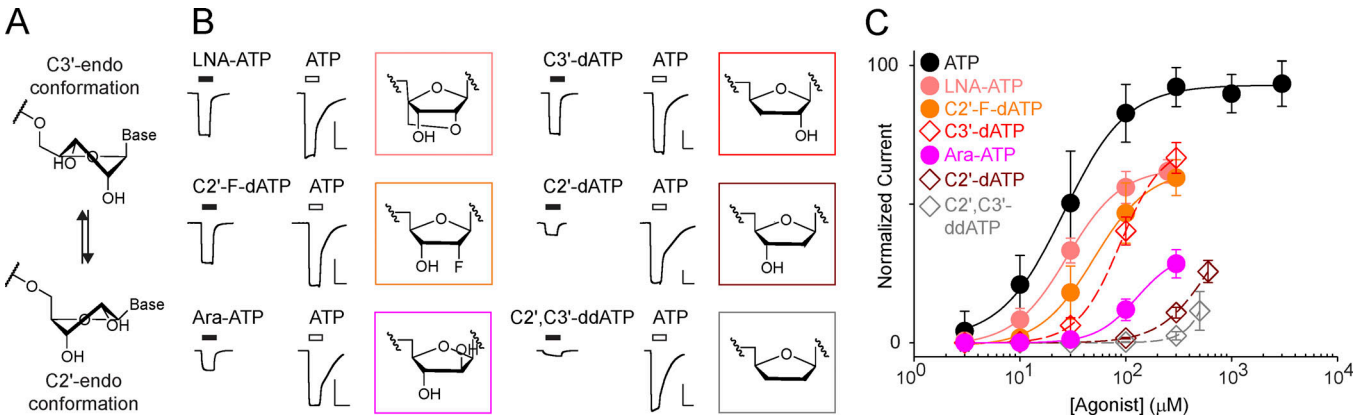

Figure 7. **Probing the effects of sugar modification on ligand recognition. (A)** Scheme of possible sugar pucker conformations: C3′-endo ribose conformation with C3′-hydroxyl group puckered in the endo face (upper panel) and C2′-endo ribose conformation (C2′-hydroxyl group puckered in the endo face; lower panel). **(B)** Peak current recorded in response to the highest tested concentration of sugar-modified nucleoside triphosphate analogues (chemical base structures shown in frames) compared with that elicited by 1 mM of ATP. Bars, x, 12 s; y, 2 µA. **(C)** ATP-elicited concentration–response data for sugar-modified analogues, normalized to current elicited by 1 mM of ATP (mean ± SD; *n* = 4–9).

To test whether increasing the rigidity by conformationally locking the ribose would alter apparent affinity or efficacy, we employed LNA-ATP (Campbell and Wengel, 2011; Fig. 7 B), which locks the ribose into the C3′-endo conformation due to a methylene bridge between the C2′ oxygen and the C4′ carbon. Indeed, LNA-ATP elicited robust currents at P2X2Rs, with an apparent affinity indistinguishable from ATP, although with significantly reduced efficacy (Fig. 7 C and Table 5). This result was similar to that obtained with C2′-F-dATP, which can interconvert between the two sugar pucker conformations, but has a preference for the C3′-endo ribose conformation: the EC_{50} was only twofold higher than that for ATP and, similar to LNA-ATP, the efficacy was reduced to ∼60% (Fig. 7, B and C; and Table 5). Together, this suggests that biasing the sugar pucker conformation toward C3′-endo reduces efficacy without major effects on apparent affinity. By contrast, a sugar analogue favoring the C2′-endo conformation, Ara-ATP showed both lower apparent affinity than ATP (EC_{50} could not be determined precisely, but is >100 µM) and greatly reduced efficacy (Fig. 7, B and C; and Table 5). We were unable to obtain an analogue of ATP locked into the C2′-endo conformation, but our data are consistent with the notion of the relative distribution of sugar pucker conformations being important for agonist apparent affinity and efficacy.

We next turned to a range of C2′ and/or C3′ substituted ribose analogues. This demonstrated that, similar to results obtained with the P2X1R (Fryatt et al., 2016), removing the C3′ hydroxyl (C3′-dATP) only has a modest effect on apparent affinity and efficacy (threefold increase in EC_{50}, ∼30% reduction in efficacy), while a lack of the C2′ hydroxyl on the sugar (C2′-dATP) requires much higher concentrations to activate P2X2Rs (EC_{50} > 300 µM). Consistent with these findings, the removal of both hydroxyl groups (C2′-C3′-ddATP) resulted in an even less potent agonist (Fig. 7, B and C; and Table 5).

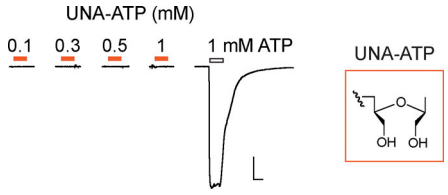

Figure 8. **UNA-ATP does not elicit macroscopic current responses.** Left: Currents elicited by increasing concentrations of UNA-ATP (orange lines) compared with application of 1 mM ATP to the same cell. Bars, x, 10 s; y, 1 µA. Right: Chemical structure of UNA-ATP; note the lack of a covalent bond between the C2′ and C3′ ring positions, which makes the analogue highly flexible.

P2X2R single channel behavior in the presence of different agonists

Finally, we wanted to assess if the chemical nature and/or binding pose of the ligand would affect the conformational landscape in the pore domain. Interestingly, single channel recordings of P2X2Rs are known to exhibit a characteristic open state flickering behavior (Evans, 1996; Ding and Sachs, 1999; Habermacher et al., 2016), which is likely to originate from transitions between multiple short-lived open states. Here, we thus wanted to address the question of whether the relative occupancy of these open states is influenced by the ligand structure, e.g., if subtly altered agonist binding poses might affect the relative occupancy of the different open states. Specifically, we sought to test if unitary current or the degree of open state flicker is affected by a subset of base-modified nucleoside triphosphates (ATP versus CTP, GTP, and UTP) or ATP analogues with different propensities for sugar pucker conformations (ATP versus LNA-ATP, C2′-F-dATP, and Ara-ATP). We therefore performed single channel recordings from outside-out patches excised from human embryonic kidney (HEK) cells expressing rP2X2-3T receptors (Li et al., 2008) and applied subsaturating concentrations of ATP, CTP, GTP, UTP, LNA-ATP, C2′-F-dATP, or Ara-ATP. To readily detect single channel currents, we chose to express rP2X2-3T, which is a

Table 5. **Concentration–response data for different sugar-modified agonists**

Agonist	EC_{50} (μM)	n_H	$I_{max\ agonist}/I_{max\ ATP}$ (%)	*n*
ATP	32 ± 4	1.4 ± 0.1	n/a	15
LNA-ATP	27 ± 1	1.8 ± 0.1	66 ± 1	9
C2′-F-dATP	52 ± 6**	2.1 ± 0.1***	60 ± 2	8
Ara-ATP	>100	ND	ND	6
C3′-dATP	83 ± 4****	2.6 ± 0.1****	67 ± 2	8
C2′-dATP	>300	ND	ND	9
C2′-C3′-ddATP	ND	ND	ND	ND

Concentration–response data (EC_{50}) and Hill coefficient (n_H) for ATP and a range of sugar-modified nucleoside triphosphate analogues (shown as mean ± SEM). Relative efficacy expressed as maximal current compared to that elicited by 1 mM of ATP and number of experiments (*n*) and are also shown (n/a: not applicable; ND, not determined). Significant differences were determined by one-way ANOVA with Dunnett's test. **, P < 0.01; ***, P = 0.0001; ****, P < 0.0001.

modified version of the rP2X2 receptor known to be similar to WT in terms of ATP-elicited concentration–response relationships (Li et al., 2008), while displaying higher ATP-induced unitary currents (Habermacher et al., 2016). We then analyzed the resulting single channel openings to obtain (a) the unitary current and (b) the degree of open state flicker (expressed as SD of the open state amplitude [SD_{open}] or relative SD to unitary current [relative SD]). However, we found that none of the tested agonists had a significant effect on either of the parameters (Fig. 9 and Table 6).

Discussion

In this study, we complemented amide-to-ester substitutions in the P2X2R binding pocket with testing of a range of subtle nucleoside triphosphate analogues to systematically decipher the molecular determinants for ligand recognition and discrimination in P2X2Rs. To the best of our knowledge, this is the first study using noncanonical amino acids in P2XRs.

Sugar pucker conformation is a major determinant in agonist recognition

Recent structures of ATP-bound P2XRs have indicated that ATP is likely to bind in a U-shaped conformation with surprisingly few contacts between the ATP ribose moiety and proximal residues of the receptor protein (Hattori and Gouaux, 2012; Kasuya et al., 2016; Mansoor et al., 2016). Supporting this notion, it has previously been shown that even large C2′/C3′ ribose substituents, such as in Alexa Fluor 647–ATP, 2′-(3′)-*O*-(2,4,6-trinitrophenyl) adenosine 5′-triphosphate, or 2′-(3′)-*O*-(4-benzoylbenzoyl) adenosine 5′-triphosphate, are still capable of activating P2XRs (Khakh and North, 2012; Bhargava et al., 2013). However, another study on P2X2Rs has recently pointed at crucial contributions of both the C2′ and C3′ ribose hydroxyl groups and suggested that the former contribute to an intramolecular H-bond with the γ-phosphate group (Fryatt et al., 2016). Indeed, we find that while the removal of the C3′ hydroxyl (C3′-dATP) shifts the EC_{50} about threefold and reduces efficacy by ∼30%, removing the 2′ hydroxyl (C2′-dATP) decreases apparent affinity ≥10-fold (efficacy could not be determined). Removal of both C2′ and C3′ hydroxyl groups (C2′-C3′-ddATP) further decreased apparent affinity and efficacy. However, substituting the (arguably more important) C2′ hydroxyl with a fluorine (C2′-F-dATP) is well tolerated, with the apparent affinity decreased only twofold and efficacy reduced by ∼40%. This is somewhat surprising, as C2′-F-dATP contains a C2′ fluorine and displays a preference for the C3′-endo ribose conformation, both of which disfavor the previously proposed intramolecular H-bonds between the sugar C2′ substituent and the γ-phosphate group (Fryatt et al., 2016). Additionally, an analogue of ATP permanently locked into the C3′-endo conformation (LNA-ATP) displayed ATP-like apparent affinity and only a minor decrease in efficacy. Altogether, this raises the possibility that it is the sugar pucker conformation (which determines the relative position/angle between phosphate tail and base moiety; Fig. 7 A), rather than propensity for intramolecular H-bonds, that is important for agonist recognition. Indeed, an analogue favoring the C2′-endo conformation, which would be expected to strengthen the putative intramolecular H-bond, Ara-ATP, shows greatly reduced efficacy and apparent affinity. Further support for this notion stems from the fact that C2′-dATP, favoring the C2′-endo conformation, has a much more pronounced effect than C3′-dATP, which has a preference for the C3′-endo conformation. Additionally, and despite preserving both the C2′ and the C3′ hydroxyls, UNA-ATP, which lacks a covalent bond between the C2′ and C3′ sugar positions, did not act as an agonist on P2X2Rs. We attribute this to UNA-ATP being unable to establish a relative position/angle of phosphate tail and base moiety that would allow them to fit into the P2XR binding pocket.

In conclusion, our data support the notion that the ATP sugar component, possibly in addition to the intramolecular H-bond formation with the γ-phosphate group, optimally positions the phosphate and base components into the binding pocket via its intrinsic equilibrium between sugar pucker conformations. If a similar pattern holds true in other P2XR subtypes, this might aid the future design of more (subtype-) specific P2XR ligands with C2′/C3′ substituents.

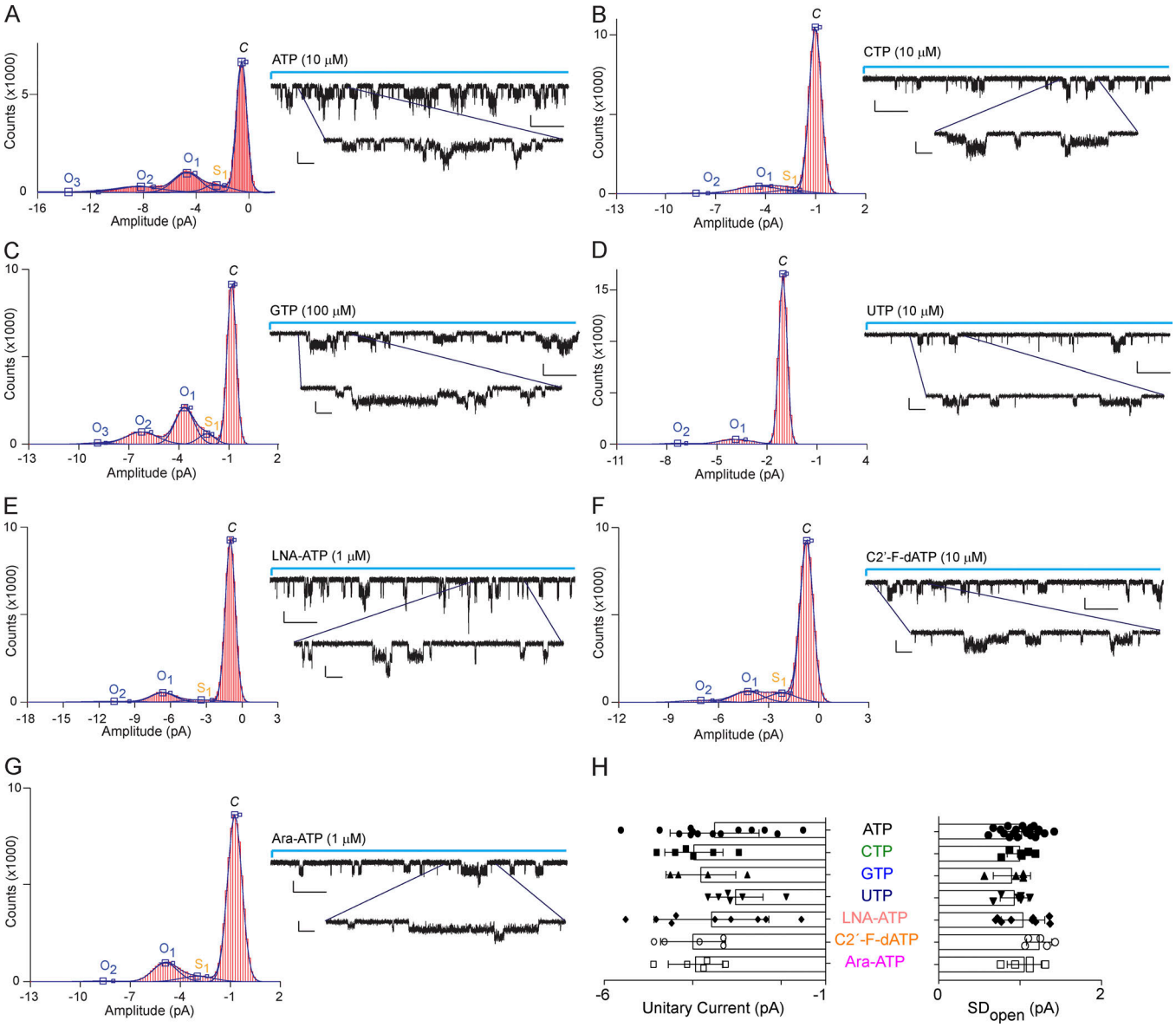

Figure 9. **Single channel current amplitude and flicker are independent of agonist structure. (A–G)** Left panels: Example of all-point histograms fitted by a sum of Gaussian distributions; *c* represents the closed channel; O_1, full-conductance open state; O_2 and O_3, full-conductance open state of two, three, or more channels open simultaneously; and S_1, subconductance state. The histograms are obtained from the current analysis of the patch shown on the right (note leak current was not subtracted for histogram visualization). Right panels: Examples of single channel currents from excised outside-out patches expressing rP2X2-3T receptors. Channel openings (downward deflections) were elicited by application of different agonists for 10 s (indicated by light blue line). Bars, x, 1 s; y, 5 pA; insets, x, 0.1 s; y, 5 pA. **(H)** Mean ± SD of unitary current amplitudes (left) and SD_{open} (right; n = 4–20; two to five sweeps were averaged for each patch). Concentrations used: ATP (1 μM), CTP (10 μM), GTP (100 μM), UTP (10 μM), LNA-ATP (1 μM), C2′-F-dATP (10 μM), and Ara-ATP (1 μM).

Ligand discrimination arises primarily through Thr184-mediated interactions

Our results highlight the differential effects of mutating the conserved basic side chains lining the ATP-binding site: while in the case of Lys69 and Lys308 side chain charge as well as steric/H-bonding patterns are important, Lys188 is mostly contributing with its charge/ability to act as a H-bond donor (Fig. 3). This is likely due to the interaction of Lys188 with the α-phosphate of ATP via a water molecule (Hattori and Gouaux, 2012) being less susceptible to steric effects than alterations at Lys69, Lys71, Arg290, and Lys308, which are more closely packed around the ligand molecule. Interestingly, mutations at Lys71 and Arg290 yielded more ambiguous results, as in both cases removal of charge (i.e., Gln mutation) is detrimental to ATP sensitivity, while charge-retaining mutations result in intermediate phenotypes (Lys71Arg and Arg290Lys, respectively). In both cases, this is likely to indicate that while charge clearly plays an important role, steric components and/or H-bonding patterns are also crucial to ligand recognition. However, relative effects of changes in sterics or H-bonding pattern cannot be discriminated using conventional approaches and therefore awaits further investigation in the future.

Table 6. **Single channel parameters for different agonists**

Agonist	Unitary current (pA)	SD_{open}	Relative SD	*n*
ATP	−3.51 ± 0.2	1.02 ± 0.1	0.32 ± 0.03	20
CTP	−3.98 ± 0.3	0.99 ± 0.1	0.25 ± 0.01	6
GTP	−3.82 ± 0.4	0.90 ± 0.1	0.23 ± 0.02	4
UTP	−3.04 ± 0.3	0.93 ± 0.1	0.31 ± 0.02	6
LNA-ATP	−3.58 ± 0.4	1.03 ± 0.1	0.32 ± 0.04	9
C2′-F-dATP	−4.00 ± 0.3	1.23 ± 0.1	0.31 ± 0.03	5
Ara-ATP	−3.94 ± 0.3	1.05 ± 0.1	0.27 ± 0.03	5

Unitary channel current, SD_{open}, and relative SD (calculated as SD_{open}/unitary current) are shown (mean ± SEM) for selected agonists, along with the number of experiments (*n*). Concentrations used: ATP (1 µM), CTP (10 µM), GTP (100 µM), UTP (10 µM), LNA-ATP (1 µM), C2′-F-dATP (10 µM), and Ara-ATP (1 µM).

In addition to the clear requirement for a positive charge in the side chain of Lys69, recent structural work (Hattori and Gouaux, 2012; Kasuya et al., 2016; Mansoor et al., 2016) had suggested that the backbone carbonyl oxygen of Lys69 forms an H-bond with the C6-amine of the ATP purine base. Similarly, the conserved Thr184 had previously been suggested to contribute to ligand binding via both its side chain and its backbone carbonyl oxygen (Jiang et al., 2000; Roberts et al., 2008; Hattori and Gouaux, 2012; Kasuya et al., 2017). However, a functional verification of the notion of Lys69 and Thr184 contributing to ligand recognition via their backbone carbonyl oxygens had not been possible because site-directed mutagenesis does not allow backbone alterations (other than the introduction of Pro, which lacks a backbone NH moiety; Sereikaitė et al., 2018). Here, we thus turned to the nonsense suppression method to incorporate amide-to-ester mutations, constituting the first use of this approach in P2XRs. The results show that the Lys69 backbone carbonyl oxygen only makes a modest contribution to agonist recognition (Val70Vah increasing the EC_{50} only four- and five-fold for ATP and CTP, respectively) and, in light of the almost identical relative change in apparent affinity for ATP and CTP, makes no contribution to ligand discrimination. By contrast, the equivalent mutation at Thr184 (Ile185Vah) reduced ATP sensitivity to a greater extent than CTP sensitivity (20- versus 8-fold increase in EC_{50}), indicating that the Thr184 backbone carbonyl oxygen contributes to ligand discrimination. This notion was further corroborated by our finding that the Thr184Val mutation reduced ATP apparent affinity slightly more than CTP apparent affinity (100- versus 30-fold increase in EC_{50}). Together, this suggests that while the backbone carbonyl oxygens of both Lys69 and Thr184 contribute to ligand recognition, ligand discrimination is mediated by a combination of the side chain hydroxyl and the backbone carbonyl oxygen of Thr184. This is in slight contrast to recent structural data on zfP2X4 (Kasuya et al., 2017), which had predicted the backbone carbonyl oxygen of Lys69 and Thr184 (Lys70 and Thr189 in zfP2X4) to be positioned roughly equidistant to the C6 and C4 amine substituents of ATP and CTP, respectively. Instead, the authors had suggested ligand discrimination between ATP and CTP to primarily arise from different distances to the side chains of Thr184 and Gln138 (which is Arg143 in zfP2X4). However, in light of our functional data and the fact that Gln138 is not conserved throughout different P2XRs isoforms (Kawate et al., 2009), we suggest ligand discrimination to arise from side chain and backbone interactions mediated by Thr184, although Gln138 (P2X2)/Arg143 (zfP2X4) are likely to contribute to subtype-specific differences. This hypothesis is further supported by (a) our finding that mutating the backbone carbonyl oxygen of Lys69 has similar effects on the apparent affinity of ATP and CTP and (b) the fact that the known physiologically relevant P2XR agonists differ in only their base component, which in turn has been shown to be relatively inert to even bulky substituents at the 8 position of ATP (Jiang et al., 2011), leaving the more distal moieties of the base component (N1- and N3-nitrogens and C6- and C4-substituents of purines and pyrimidines, respectively) to be crucial for ligand discrimination. The notion of the more distal moieties of the base components being important is further supported by our mutagenesis data on sites predicted to interact with the C6- and N1-positions of ATP and the C3- and N4-positions of CTP, respectively (i.e., side chain and backbone carbonyl oxygen of Thr184) and the observation that adding C2-substituents to purine bases (isoGTP) is detrimental to agonist apparent affinity.

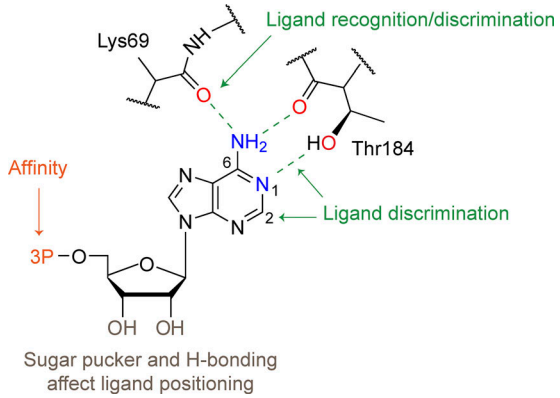

Figure 10. **Cartoon summary of the key findings.** Note that this study focused on conserved side chains only. Other factors are likely to also contribute to ligand recognition and discrimination.

Nucleoside triphosphate analogues support the role of Thr184 in ligand discrimination

Our above findings are complemented by the results obtained with different nucleoside triphosphate analogues, although we could not apply all ligands at high (millimolar) concentrations, preventing us from obtaining a more complete dataset. However, and regardless of whether we used nucleoside triphosphate analogues with purine or pyrimidine bases, we find that introducing purine C2-substituents and/or altering purine C6- or the equivalent pyrimidine C4-substituents have drastic effects on both apparent affinity and efficacy.

Comparison among both purines (ATP versus ITP) and pyrimidines (CTP versus UTP) shows that exchanging the amine substituent in the equivalent C6- and C4-position of purines and pyrimidines (i.e., ATP and CTP) for an oxygen (ITP and UTP, respectively) results in both apparent affinity and efficacy being significantly reduced. These findings can be easily rationalized in light of the importance of the H-bonds originating from the Lys69 and Thr184 backbone carbonyl atoms, as this would result in electrostatic dipole repulsion between the protein backbone and the double-bonded oxygen of the ligand (C6 in purines and C4 in pyrimidines).

Similarly, introducing a C2-substituent in purine bases (i.e., isoGTP and GTP) lowered apparent affinity to the millimolar range. However, neither compound could be fully assessed in terms of its efficacy, so further conclusions about possible effects through introduction of these substituents on agonist efficacy are precluded. However, CTP (which also contains a C2-substituent) shows ATP-like efficacy, suggesting that introduction of C2-substituents is detrimental in the case of purine bases, but not for the smaller pyrimidine bases.

Indeed, our data show that while pyrimidine-derived agonists can still yield ATP-like efficacy (e.g., CTP), agonists containing less bulky bases, such as CTP and UTP, result in greatly increased EC_{50} values. This is likely due to the increased distance to both the backbone carbonyl oxygen and side chain hydroxyl of Thr184. Overall, these findings further support the notion that it is this part of the ligand–protein interaction that is an important determinant for ligand discrimination. However, this might differ for some intermediate activation states, which can show altered agonist selectivity profiles (Browne and North, 2013).

Open channel flicker is unaffected by chemical nature of orthosteric ligands

P2XRs display a characteristic open state flicker behavior (Evans, 1996; Ding and Sachs, 1999; Habermacher et al., 2016), likely due to rapid transitions between multiple open states. Interestingly, recent structural and functional work on other ligand-gated ion channels, such as transient-receptor potential channels and serotonin-gated 5-hydroxytryptamine receptors, has shown that a single agonist as well as two different ones can evoke distinct channel open states (Cao et al., 2013; Basak et al., 2018; Canul-Sánchez et al., 2018; Polovinkin et al., 2018; Zubcevic et al., 2018). Because our above results, as well as previous data (Jiang et al., 2011), suggest that ATP alone and ATP-like agonists can adopt different binding poses within the orthosteric binding site, we wanted to assess if any the different agonists tested here were able to bias the P2X2R toward a particular open state (or subset of open states). However, we found that neither the unitary current nor the degree of open channel flicker is dependent on the exact chemical nature of the ligand. In other words, slightly altered binding poses in the orthosteric binding pocket are unlikely to change the relative occupancy of open states of P2X2Rs.

Conclusions

By combining subtle alterations of both the P2X2R binding site and its primary agonist ATP, we provide experimental evidence that backbone-mediated interactions are important for ligand recognition and discrimination. Specifically, we identify interactions between the N1 (N3), C2, and C6 (C4) positions of purine (pyrimidine) bases and the protein backbone carbonyl oxygens of Lys69 and Thr184, as well as the hydroxyl side chain of Thr184, as important for ligand recognition and discrimination. Together, our data suggest an intriguingly simple but highly asymmetric model for ligand discrimination by conserved elements in P2XRs: the phosphate tail engages in tight but non-discriminatory interactions that are conserved across all nucleoside triphosphates, while changes in ligand affinity and efficacy are primarily mediated through alterations in base–protein interactions (Fig. 10). Importantly, the precise orientation/fit of the base is primarily dictated by the sugar pucker conformation.

Acknowledgments

The authors would like to thank Dr. Mahboubi Harkat and Sarune Bielickaite for technical assistance and Drs. M.H. Poulsen and K.K. Khoo for comments on the manuscript.

We acknowledge the Lundbeck Foundation (R139-2012-12390 to S.A. Pless), Carlsberg Foundation (2013-01-0439 to S.A. Pless), Beckett Foundation (39414/42389 to S.A. Pless), Hartmann Foundation (R73-A27283 to S.A. Pless), Hørslev Foundation (203866 to S.A. Pless), and Agence Nationale de la Recherche (ANR-14-CE11-0004-01 to T. Grutter) for support.

The authors declare no competing financial interests.

Author contributions: F. Gasparri conducted all experiments. J. Wengel contributed reagents. F. Gasparri, T. Grutter, and S.A. Pless designed experiments and analyzed data. The manuscript was written through contributions of all authors. All authors have given approval to the final version of the manuscript.

Kenton J. Swartz served as editor.

Submitted: 14 February 2019
Accepted: 6 May 2019

References

Arulkumaran, N., R.J. Unwin, and F.W. Tam. 2011. A potential therapeutic role for P2X7 receptor (P2X7R) antagonists in the treatment of inflammatory diseases. *Expert Opin. Investig. Drugs.* 20:897–915. https://doi.org/10.1517/13543784.2011.578068

Basak, S., Y. Gicheru, S. Rao, M.S.P. Sansom, and S. Chakrapani. 2018. Cryo-EM reveals two distinct serotonin-bound conformations of full-length 5-HT_{3A} receptor. *Nature.* 563:270–274. https://doi.org/10.1038/s41586-018-0660-7

Bhargava, Y., A. Nicke, and J. Rettinger. 2013. Validation of Alexa-647-ATP as a powerful tool to study P2X receptor ligand binding and desensitization. *Biochem. Biophys. Res. Commun.* 438:295–300. https://doi.org/10.1016/j.bbrc.2013.07.058

Broom, D.C., D.J. Matson, E. Bradshaw, M.E. Buck, R. Meade, S. Coombs, M. Matchett, K.K. Ford, W. Yu, J. Yuan, et al. 2008. Characterization of N-(adamantan-1-ylmethyl)-5-[(3R-amino-pyrrolidin-1-yl)methyl]-2-chloro-benzamide, a P2X7 antagonist in animal models of pain and inflammation. *J. Pharmacol. Exp. Ther.* 327:620–633. https://doi.org/10.1124/jpet.108.141853

Browne, L.E., and R.A. North. 2013. P2X receptor intermediate activation states have altered nucleotide selectivity. *J. Neurosci.* 33:14801–14808. https://doi.org/10.1523/JNEUROSCI.2022-13.2013

Burnstock, G. 2007. Physiology and pathophysiology of purinergic neurotransmission. *Physiol. Rev.* 87:659–797. https://doi.org/10.1152/physrev.00043.2006

Campbell, M.A., and J. Wengel. 2011. Locked vs. unlocked nucleic acids (LNA vs. UNA): contrasting structures work towards common therapeutic goals. *Chem. Soc. Rev.* 40:5680–5689. https://doi.org/10.1039/c1cs15048k

Canul-Sánchez, J.A., I. Hernández-Araiza, E. Hernández-García, I. Llorente, S.L. Morales-Lázaro, L.D. Islas, and T. Rosenbaum. 2018. Different agonists induce distinct single-channel conductance states in TRPV1 channels. *J. Gen. Physiol.* 150:1735–1746. https://doi.org/10.1085/jgp.201812141

Cao, E., M. Liao, Y. Cheng, and D. Julius. 2013. TRPV1 structures in distinct conformations reveal activation mechanisms. *Nature.* 504:113–118. https://doi.org/10.1038/nature12823

Carter, D.S., M. Alam, H. Cai, M.P. Dillon, A.P. Ford, J.R. Gever, A. Jahangir, C. Lin, A.G. Moore, P.J. Wagner, and Y. Zhai. 2009. Identification and SAR of novel diaminopyrimidines. Part 1: The discovery of RO-4, a dual P2X(3)/P2X(2/3) antagonist for the treatment of pain. *Bioorg. Med. Chem. Lett.* 19:1628–1631. https://doi.org/10.1016/j.bmcl.2009.02.003

Chataigneau, T., D. Lemoine, and T. Grutter. 2013. Exploring the ATP-binding site of P2X receptors. *Front. Cell. Neurosci.* 7:273. https://doi.org/10.3389/fncel.2013.00273

Coddou, C., Z. Yan, T. Obsil, J.P. Huidobro-Toro, and S.S. Stojilkovic. 2011. Activation and regulation of purinergic P2X receptor channels. *Pharmacol. Rev.* 63:641–683. https://doi.org/10.1124/pr.110.003129

Dahan, D.S., M.I. Dibas, E.J. Petersson, V.C. Auyeung, B. Chanda, F. Bezanilla, D.A. Dougherty, and H.A. Lester. 2004. A fluorophore attached to nicotinic acetylcholine receptor beta M2 detects productive binding of agonist to the alpha delta site. *Proc. Natl. Acad. Sci. USA.* 101:10195–10200. https://doi.org/10.1073/pnas.0301885101

Ding, S., and F. Sachs. 1999. Single channel properties of P2X2 purinoceptors. *J. Gen. Physiol.* 113:695–720. https://doi.org/10.1085/jgp.113.5.695

England, P.M., Y. Zhang, D.A. Dougherty, and H.A. Lester. 1999. Backbone mutations in transmembrane domains of a ligand-gated ion channel: implications for the mechanism of gating. *Cell.* 96:89–98. https://doi.org/10.1016/S0092-8674(00)80962-9

Ennion, S., S. Hagan, and R.J. Evans. 2000. The role of positively charged amino acids in ATP recognition by human P2X(1) receptors. *J. Biol. Chem.* 275:29361–29367. https://doi.org/10.1074/jbc.M003637200

Evans, R.J. 1996. Single channel properties of ATP-gated cation channels (P2X receptors) heterologously expressed in Chinese hamster ovary cells. *Neurosci. Lett.* 212:212–214. https://doi.org/10.1016/0304-3940(96)12804-4

Freist, W., J.F. Verhey, W. Stühmer, and D.H. Gauss. 1998. ATP binding site of P2X channel proteins: structural similarities with class II aminoacyl-tRNA synthetases. *FEBS Lett.* 434:61–65. https://doi.org/10.1016/S0014-5793(98)00958-2

Fryatt, A.G., S. Dayl, P.M. Cullis, R. Schmid, and R.J. Evans. 2016. Mechanistic insights from resolving ligand-dependent kinetics of conformational changes at ATP-gated P2X1R ion channels. *Sci. Rep.* 6:32918. https://doi.org/10.1038/srep32918

Habermacher, C., A. Martz, N. Calimet, D. Lemoine, L. Peverini, A. Specht, M. Cecchini, and T. Grutter. 2016. Photo-switchable tweezers illuminate pore-opening motions of an ATP-gated P2X ion channel. *eLife.* 5:e11050. https://doi.org/10.7554/eLife.11050

Hattori, M., and E. Gouaux. 2012. Molecular mechanism of ATP binding and ion channel activation in P2X receptors. *Nature.* 485:207–212. https://doi.org/10.1038/nature11010

Hausmann, R., J. Günther, A. Kless, D. Kuhlmann, M.U. Kassack, G. Bahrenberg, F. Markwardt, and G. Schmalzing. 2013. Salt bridge switching from Arg290/Glu167 to Arg290/ATP promotes the closed-to-open transition of the P2X2 receptor. *Mol. Pharmacol.* 83:73–84. https://doi.org/10.1124/mol.112.081489

Hausmann, R., A. Kless, and G. Schmalzing. 2015. Key sites for P2X receptor function and multimerization: overview of mutagenesis studies on a structural basis. *Curr. Med. Chem.* 22:799–818. https://doi.org/10.2174/0929867322666141128163215

Hechler, B., S. Magnenat, M.L. Zighetti, M.U. Kassack, H. Ullmann, J.P. Cazenave, R. Evans, M. Cattaneo, and C. Gachet. 2005. Inhibition of platelet functions and thrombosis through selective or nonselective inhibition of the platelet P2 receptors with increasing doses of NF449 [4,4′,4″,4‴-(carbonylbis(imino-5,1,3-benzenetriylbis-(carbonylimino)))tetrakis-benzene-1,3-disulfonic acid octasodium salt]. *J. Pharmacol. Exp. Ther.* 314:232–243. https://doi.org/10.1124/jpet.105.084673

Honore, P., D. Donnelly-Roberts, M.T. Namovic, G. Hsieh, C.Z. Zhu, J.P. Mikusa, G. Hernandez, C. Zhong, D.M. Gauvin, P. Chandran, et al. 2006. A-740003 [N-(1-[(cyanoimino)(5-quinolinylamino) methyl]amino-2,2-dimethylpropyl)-2-(3,4-dimethoxyphenyl)acetamide], a novel and selective P2X7 receptor antagonist, dose-dependently reduces neuropathic pain in the rat. *J. Pharmacol. Exp. Ther.* 319:1376–1385. https://doi.org/10.1124/jpet.106.111559

Jarvis, M.F., E.C. Burgard, S. McGaraughty, P. Honore, K. Lynch, T.J. Brennan, A. Subieta, T. Van Biesen, J. Cartmell, B. Bianchi, et al. 2002. A-317491, a novel potent and selective non-nucleotide antagonist of P2X3 and P2X2/3 receptors, reduces chronic inflammatory and neuropathic pain in the rat. *Proc. Natl. Acad. Sci. USA.* 99:17179–17184. https://doi.org/10.1073/pnas.252537299

Jiang, L.H., F. Rassendren, A. Surprenant, and R.A. North. 2000. Identification of amino acid residues contributing to the ATP-binding site of a purinergic P2X receptor. *J. Biol. Chem.* 275:34190–34196. https://doi.org/10.1074/jbc.M005481200

Jiang, R., A. Martz, S. Gonin, A. Taly, L.P. de Carvalho, and T. Grutter. 2010. A putative extracellular salt bridge at the subunit interface contributes to the ion channel function of the ATP-gated P2X2 receptor. *J. Biol. Chem.* 285:15805–15815. https://doi.org/10.1074/jbc.M110.101980

Jiang, R., D. Lemoine, A. Martz, A. Taly, S. Gonin, L. Prado de Carvalho, A. Specht, and T. Grutter. 2011. Agonist trapped in ATP-binding sites of the P2X2 receptor. *Proc. Natl. Acad. Sci. USA.* 108:9066–9071. https://doi.org/10.1073/pnas.1102170108

Karasawa, A., and T. Kawate. 2016. Structural basis for subtype-specific inhibition of the P2X7 receptor. *eLife.* 5:e22153. https://doi.org/10.7554/eLife.22153

Kasuya, G., Y. Fujiwara, M. Takemoto, N. Dohmae, Y. Nakada-Nakura, R. Ishitani, M. Hattori, and O. Nureki. 2016. Structural Insights into Divalent Cation Modulations of ATP-Gated P2X Receptor Channels. *Cell Reports.* 14:932–944. https://doi.org/10.1016/j.celrep.2015.12.087

Kasuya, G., Y. Fujiwara, H. Tsukamoto, S. Morinaga, S. Ryu, K. Touhara, R. Ishitani, Y. Furutani, M. Hattori, and O. Nureki. 2017. Structural insights into the nucleotide base specificity of P2X receptors. *Sci. Rep.* 7:45208. https://doi.org/10.1038/srep45208

Kawate, T., J.C. Michel, W.T. Birdsong, and E. Gouaux. 2009. Crystal structure of the ATP-gated P2X(4) ion channel in the closed state. *Nature.* 460:592–598. https://doi.org/10.1038/nature08198

Khakh, B.S., and R.A. North. 2012. Neuromodulation by extracellular ATP and P2X receptors in the CNS. *Neuron.* 76:51–69. https://doi.org/10.1016/j.neuron.2012.09.024

Lazarowski, E.R., R.C. Boucher, and T.K. Harden. 2003. Mechanisms of release of nucleotides and integration of their action as P2X- and P2Y-receptor activating molecules. *Mol. Pharmacol.* 64:785–795. https://doi.org/10.1124/mol.64.4.785

Li, M., T.H. Chang, S.D. Silberberg, and K.J. Swartz. 2008. Gating the pore of P2X receptor channels. *Nat. Neurosci.* 11:883–887. https://doi.org/10.1038/nn.2151

Lynagh, T., V.V. Komnatnyy, and S.A. Pless. 2017. Unique Contributions of an Arginine Side Chain to Ligand Recognition in a Glutamate-gated Chloride Channel. *J. Biol. Chem.* 292:3940–3946. https://doi.org/10.1074/jbc.M116.772939

Mansoor, S.E., W. Lü, W. Oosterheert, M. Shekhar, E. Tajkhorshid, and E. Gouaux. 2016. X-ray structures define human P2X(3) receptor gating cycle and antagonist action. *Nature.* 538:66–71. https://doi.org/10.1038/nature19367

Marquez-Klaka, B., J. Rettinger, and A. Nicke. 2009. Inter-subunit disulfide cross-linking in homomeric and heteromeric P2X receptors. *Eur. Biophys. J.* 38:329–338. https://doi.org/10.1007/s00249-008-0325-9

Nowak, M.W., J.P. Gallivan, S.K. Silverman, C.G. Labarca, D.A. Dougherty, and H.A. Lester. 1998. In vivo incorporation of unnatural amino acids into ion channels in Xenopus oocyte expression system. *Methods Enzymol.* 293:504–529. https://doi.org/10.1016/S0076-6879(98)93031-2

Pless, S.A., and C.A. Ahern. 2013. Unnatural amino acids as probes of ligand-receptor interactions and their conformational consequences. *Annu. Rev. Pharmacol. Toxicol.* 53:211–229. https://doi.org/10.1146/annurev-pharmtox-011112-140343

Polovinkin, L., G. Hassaine, J. Perot, E. Neumann, A.A. Jensen, S.N. Lefebvre, P.J. Corringer, J. Neyton, C. Chipot, F. Dehez, et al. 2018. Conformational transitions of the serotonin 5-HT_3 receptor. *Nature.* 563:275–279. https://doi.org/10.1038/s41586-018-0672-3

Roberts, J.A., and R.J. Evans. 2004. ATP binding at human P2X1 receptors. Contribution of aromatic and basic amino acids revealed using mutagenesis and partial agonists. *J. Biol. Chem.* 279:9043–9055. https://doi.org/10.1074/jbc.M308964200

Roberts, J.A., and R.J. Evans. 2006. Contribution of conserved polar glutamine, asparagine and threonine residues and glycosylation to agonist action at human P2X1 receptors for ATP. *J. Neurochem.* 96:843–852. https://doi.org/10.1111/j.1471-4159.2005.03593.x

Roberts, J.A., H.R. Digby, M. Kara, S. El Ajouz, M.J. Sutcliffe, and R.J. Evans. 2008. Cysteine substitution mutagenesis and the effects of methanethiosulfonate reagents at P2X2 and P2X4 receptors support a core common mode of ATP action at P2X receptors. *J. Biol. Chem.* 283:20126–20136. https://doi.org/10.1074/jbc.M800294200

Saks, M.E., J.R. Sampson, M.W. Nowak, P.C. Kearney, F. Du, J.N. Abelson, H.A. Lester, and D.A. Dougherty. 1996. An engineered Tetrahymena tRNAGln for in vivo incorporation of unnatural amino acids into proteins by nonsense suppression. *J. Biol. Chem.* 271:23169–23175. https://doi.org/10.1074/jbc.271.38.23169

Sereikaitė, V., T.M.T. Jensen, C.R.O. Bartling, P. Jemth, S.A. Pless, and K. Strømgaard. 2018. Probing Backbone Hydrogen Bonds in Proteins by Amide-to-Ester Mutations. *ChemBioChem.* 19:2136–2145. https://doi.org/10.1002/cbic.201800350

Walker, J.E., M. Saraste, M.J. Runswick, and N.J. Gay. 1982. Distantly related sequences in the alpha- and beta-subunits of ATP synthase, myosin, kinases and other ATP-requiring enzymes and a common nucleotide binding fold. *EMBO J.* 1:945–951. https://doi.org/10.1002/j.1460-2075.1982.tb01276.x

Wilkinson, W.J., L.H. Jiang, A. Surprenant, and R.A. North. 2006. Role of ectodomain lysines in the subunits of the heteromeric P2X2/3 receptor. *Mol. Pharmacol.* 70:1159–1163. https://doi.org/10.1124/mol.106.026658

Zemkova, H., Z. Yan, Z. Liang, I. Jelinkova, M. Tomic, and S.S. Stojilkovic. 2007. Role of aromatic and charged ectodomain residues in the P2X(4) receptor functions. *J. Neurochem.* 102:1139–1150. https://doi.org/10.1111/j.1471-4159.2007.04616.x

Zhu, Y., J. Beudez, N. Yu, T. Grutter, and H.B. Zhao. 2017. P2X2 Dominant Deafness Mutations Have No Negative Effect on Wild-Type Isoform: Implications for Functional Rescue and in Deafness Mechanism. *Front. Mol. Neurosci.* 10:371. https://doi.org/10.3389/fnmol.2017.00371

Zubcevic, L., M.A. Herzik Jr., M. Wu, W.F. Borschel, M. Hirschi, A.S. Song, G.C. Lander, and S.Y. Lee. 2018. Conformational ensemble of the human TRPV3 ion channel. *Nat. Commun.* 9:4773. https://doi.org/10.1038/s41467-018-07117-w